Manganese coordination chemistry of bis(imino)phenoxide derived [2 + 2] Schiff-base macrocyclic ligands

Wenxue Yang,[a] Ke-Qing Zhao,*[a] Bi-Qin Wang,[a] Carl Redshaw,*[a,b] Mark R.J. Elsegood,*[c] Jiang-Lin Zhao[d] and Takehiko Yamato[d]

[a] *College of Chemistry and Materials Science, Sichuan Normal University, Chengdu, 610066, China.*

[b] *Department of Chemistry, The University of Hull, Cottingham Rd, Hull, HU6 7RX, U.K.*

[c] *Chemistry Department, Loughborough University, Loughborough, Leicestershire, LE11 3TU, U.K.*

[d] *Department of Applied Chemistry, Saga University, Saga, 840-8502, Japan*

E-mail: C.Redshaw@hull.ac.uk

_____

Abstract- The [2 + 2] Schiff base macrocycles $[2,2^{/}\text{-}(CH_2CH_2)(C_6H_4N)_2\text{-}2,6\text{-}(4\text{-}RC_6H_3OH)]_2$ ($\mathbf{I^RH_2}$), upon reaction with $MnCl_2$ (two equivalents) afforded the bimetallic complex $[Cl_3Mn(\mu\text{-}Cl)Mn(\mathbf{I^{Me}H_2})]$ (**1**) or the salt complex $[Cl_3Mn(NCMe)][MnCl(\mathbf{I^{tBu}H_2})]$ (**2**). Under similar conditions, use of the related [2 + 2] oxy-bridged macrocycle $[2,2^{/}\text{-}O(C_6H_4N=CH)_24\text{-}RC_6H_3OH]$ ($\mathbf{II^RH_2}$), afforded the bimetallic complexes $[(MnCl)_2\mathbf{II^R}]$ (R = Me **3**, *t*Bu **4**), whilst the macrocycle derived from 1,2-diaminobenzene and $5,5^{/}$-di-*tert*-butyl-$2,2^{/}$-dihydroxy-$3,3^{/}$-methylenedibenzaldehyde ($\mathbf{III}H_4$) afforded the complex $[(MnCl)_2(\mathbf{III})]\cdot2MeCN$ (**5·2MeCN**). For comparative studies, the salt complexes $[2,6\text{-}(ArNHCH)_2\text{-}4\text{-}MeC_6H_2O][MnCl_3(NCMe)]$ (Ar = $2,4\text{-}Me_2C_6H_3$, **6**) and $\{[2,6\text{-}(ArNHCH)\text{-}4\text{-}Me\text{-}C_6H_2O]MnCl\}_2[MnCl_4]\cdot8CH_2Cl_2$ (Ar = $4\text{-}MeC_6H_4$, **7·8CH_2Cl_2**) were prepared. The crystal structures of **1 – 7** are reported (synchrotron radiation was necessary for complexes **1**, **3** and **5**). Complexes **1 – 7** (not **5**) were screened for their potential to act as pre-catalysts for the ring opening polymerization (ROP) of ε-caprolactone; **3**, **4** and **6**, **7** were inactive, whilst **1** and **2** exhibited only poor activity with low conversion (< 15 %) at temperatures above 60 ^{o}C.

Introduction

Over the last decade, there has been a great deal of interest in the chemistry of frameworks that are capable of binding two transition metals in close proximity, due primarily to the possibilities of beneficial cooperative effects. [1] Macrocycles bearing phenoxide groups as well as accessible nitrogen centres have attracted attention, particularly from groups with biological interests, because of their controllable coordination chemistry which has allowed for the study of structure-bioactivity relationships. [2] We have previously investigated the use Schiff-base macrocycles of type IH_2, which are related to the much studied Robson-type macrocycles, [3] and have observed interesting structure/activity trends for organoaluminium complexes in the ring opening polymerization (ROP) of ε-caprolactone. [4] The metal coordination chemistry of this particular ligand set is unexplored, indeed a search of the CSD revealed no hits other than the structure of the parent pro-ligand IH_2 and a methylated derivative thereof. [5] Given this, we have initiated a programme to explore their transition metal chemistry, and have also extended our studies to include the related macrocycles IIH_2 and $IIIH_4$ (see scheme 1). We report here our initial studies on the manganese coordination chemistry of $IH_2 - IIIH_4$, and report the molecular structures of five new complexes. A search of the CSD for manganese bound in '*N,O* fashion' to a phenoxide motif bearing *ortho* imine groups revealed 116 hits. [6] We note that a number of dinuclear manganese complexes are of catalytic interest given their potential for catecholase activity, [7] whilst manganese Schiff-base complexes have also attracted attention for their antibacterial properties, [8] and have also been extensively employed in organic chemistry, for example as catalysts for asymmetric epoxidation. [9] As mentioned above, our interest stems from exploring the use of earth abundant transition metals as the metal centres in pre-catalysts for ROP, and herein, we have screened the manganese complexes for their ability to act as pre-catalysts in the ring opening polymerization (ROP) of ε-caprolactone; there is a lack of other Mn-based systems utilized in ROP of cyclic esters. [10]

2

Scheme 1

3
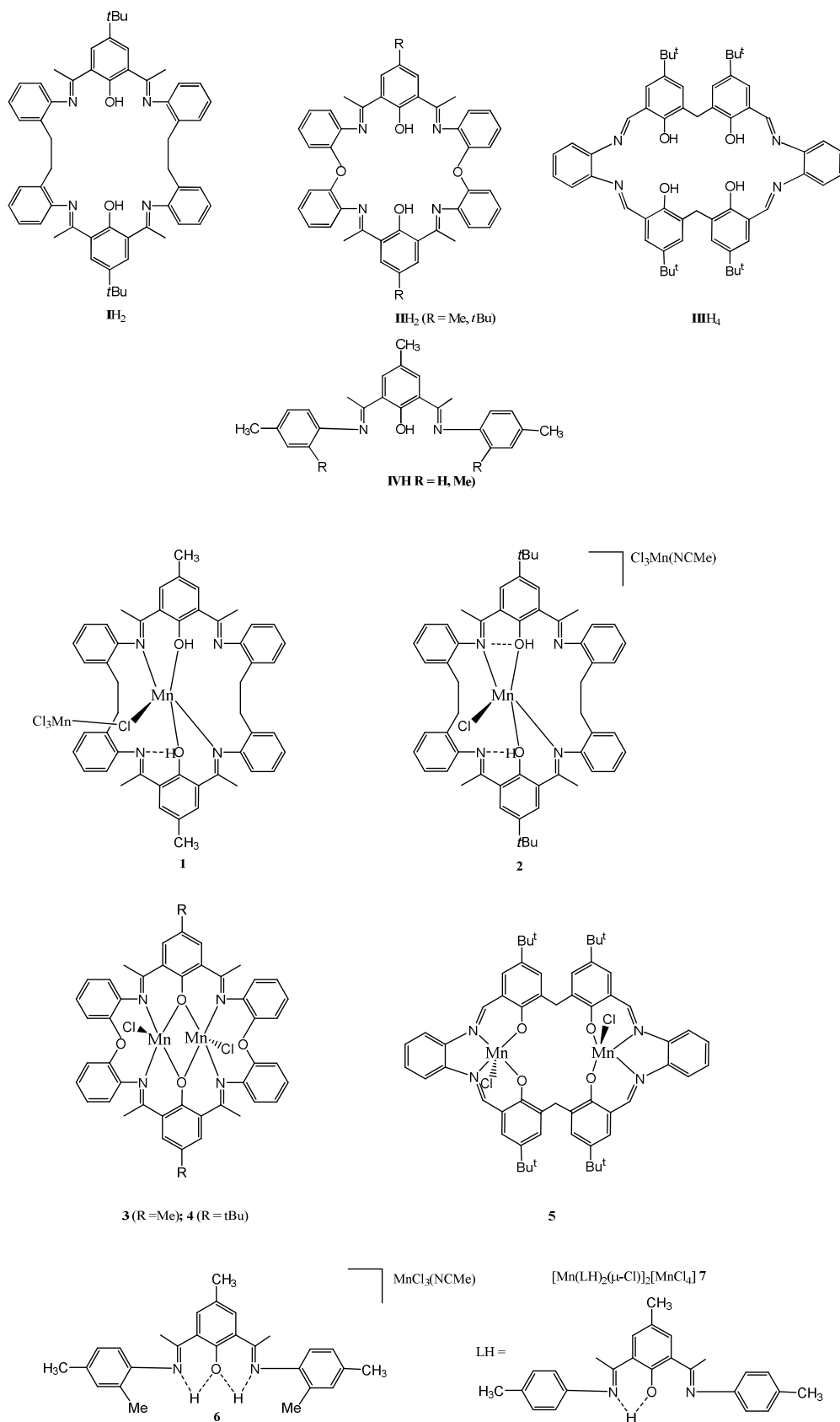
Results and Discussion

Use of {2,2$^{/}$-(CH$_2$CH$_2$)(C$_6$H$_4$NH$_2$)$_2$}

The neutral [2 + 2] macrocycle [2,2$^{/}$-(CH$_2$CH$_2$)(C$_6$H$_4$N)$_2$-2,6-(4-MeC$_6$H$_3$OH)]$_2$ (**I**^{Me}H$_2$) prepared from the

diamine {2,2$^{/}$-(CH$_2$CH$_2$)(C$_6$H$_4$NH$_2$)$_2$} and 2,6-diformyl-4-methylphenol [1,3-(CHO)$_2$-5-MeC$_6$H$_3$OH-2] in

refluxing ethanol in the presence of the Lewis acid B(OMe)$_3$, was treated with two equivalents of MnCl$_2$ in

refluxing toluene. Following work-up (see experimental), the orange complex [Cl$_3$Mn(μ-Cl)Mn(**I**^{Me})H$_2$]

(**1**) was isolated in moderate yield (*ca*. 35 %). The IR spectrum contained a strong band a 1635 cm^{-1}

assigned to v(C=N). Small crystals of **1**·3MeCN suitable for X-ray diffraction using synchrotron radiation

were grown from acetonitrile at 0 ^{o}C. The macrocycle adopts a twisted conformation to accommodate two

intramolecular H-bonds, see Figure 1 and Table S1 (ESI). The 'central' manganese [Mn(1)] possesses a

trigonal bipyramidal geometry with phenoxy oxygen atoms axial and a chloride and two imine nitrogens in

equatorial positions. The 'outer' manganese [Mn(2)] is distorted tetrahedral, and is linked to Mn(1) via a

bridging chloride [Cl(1)]. The Mn – O(phenoxide) bond lengths [2.0752(15) and 2.0954(15) Å] are slightly

shorter than the Mn^{II} – phenoxide bonds [2.1583(19) – 2.374(2) Å] observed in recently reported

mixed-valance Mn^{II}/Mn^{III} complexes of the Robson-type macrocycle derived from

2,6-diformyl-4-methylphenol and 2,2-dimethyl-1,3-diaminopropane [7b], whilst the Mn – N$_{imine}$ bond

lengths [2.1959(17) and 2.2077(19) Å] compare favourably with those observed in said mixed-valence

complexes [2.161(2) – 2.240(3) Å]. The planar section of the macrocycle from C(1) to C(14) forms a π···π

stack with an inversion related planar section on the next molecule with contacts in the range 3.29-3.51Å

(see Figure S1, ESI). In the packing of **1**·3MeCN, there are weak intermolecular interactions, e.g.

C(31)–H(31)···Cl(2) 2.61 Å (hydrogen bond geometries are given in Table S1, ESI).
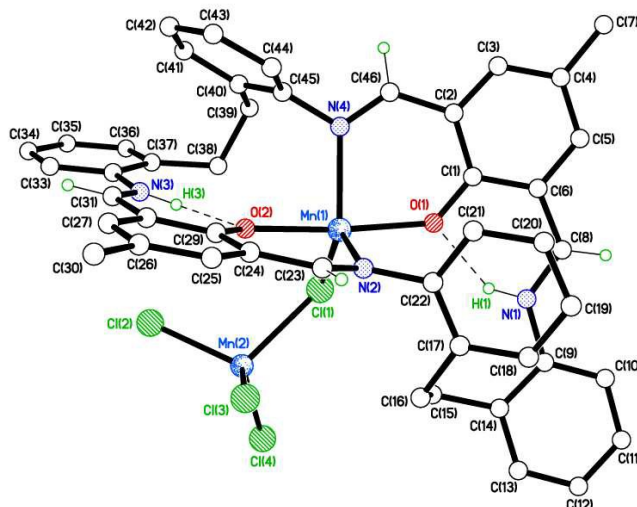
4

Figure 1. Molecular structure of [Cl$_3$Mn(μ-Cl)Mn(**I**^{Me})H$_2$] (**1**). Selected bond lengths (Å) and angles (°): Mn(1) – O(1) 2.0954(15), Mn(1) – O(2) 2.0752(15), Mn(1) – N(2) 2.1959(17), Mn(1) – N(4) 2.2077(19), Mn(1) – Cl(1) 2.4492(7), Mn(2) – Cl(1) 2.4659(7), Mn(2) – Cl(2) 2.3542(7), Mn(2) – Cl(3) 2.3430(7), Mn(2) – Cl(4) 2.3502(8); O(1) – Mn(1) – O(2) 173.94(6), Mn(1) – Cl(1) – Mn(2) 109.02(2), N(4) – Mn(1) – Cl(1) 119.39(5).

Use of the related 2,6-diformyl-4-*tert*-butylphenol [1,3-(CHO)$_2$-5-*t*BuC$_6$H$_3$OH-2] in the macrocycle synthesis under the same conditions afforded **I**^{tBu}H$_2$ and subsequent treatment with MnCl$_2$ led to the isolation of the salt complex [Cl$_3$Mn(NCMe)][MnCl(**I**^{tBu}H$_2$)] (**2**) in moderate yield (*ca.* 55 %). The IR spectrum contained a strong band a 1634 cm^{-1} assigned to *v*(C=N). Crystals suitable for X-ray diffraction were obtained from acetonitrile on prolonged standing at ambient temperature. The molecular structure is shown in Figure 2, with selected bond lengths and angles given in the caption. There is one molecule of the complex in the asymmetric unit, but no solvent of crystallization. As for **1**, one Mn ion is directly bound to the macrocycle resulting in an N$_2$O$_2$Cl trigonal bipyramidal environment (see scheme 2). The major difference from **1** is that Mn(2) is not linked to Mn(1) via a bridging chloride. The reason for this is thought to be the presence of the bulky *tert*-butyl group at the *para* position of the phenoxide of the macrocycle. However, similar to **1**, there are two intramolecular H-bonds involving the phenoxide oxygens. The Mn –

5

O(phenoxide) bond lengths in **2** [2.0712(13) and 2.0803(14) Å] and the Mn – N(imine) bond lengths [2.2359(18) and 2.2328(17) Å] are close to those observed for **1**. In **2** Mn(1) also adopts a trigonal bi-pyramidal geometry with phenoxide oxygens axial. EPR spectra for **1** and **2** recorded as powdered samples at 110 K are similar with a broad feature at around *ca*. g = 2.0, for example see Figures. S2 and S3, ESI.
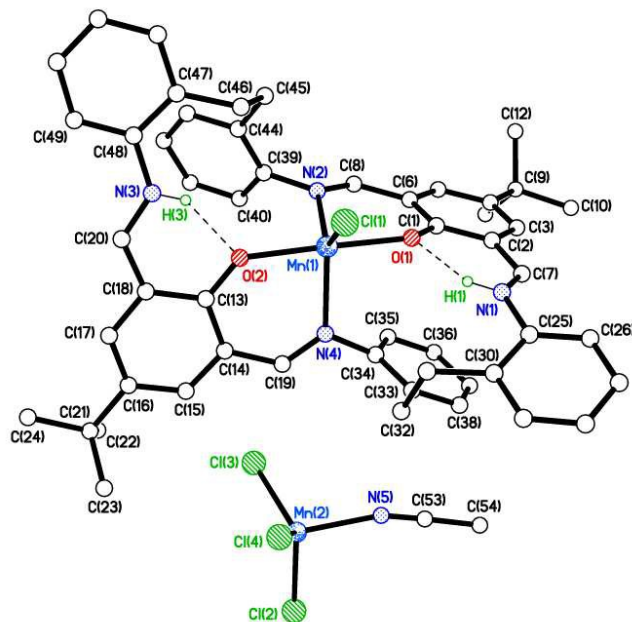
Figure 2. Molecular structure of [Cl$_3$Mn(NCMe)][MnCl(**I**^{tBu})H$_2$] (**2**). Selected bond lengths (Å) and angles (°): Mn(1) – O(1) 2.0712(13), Mn(1) – O(2) 2.0803(14), Mn(1) – N(2) 2.2359(18), Mn(1) – N(4) 2.2328(17), Mn(1) – Cl(1) 2.3860(6), Mn(2) – Cl(2) 2.3269(8), Mn(2) – Cl(3) 2.3241(7), Mn(2) – Cl(4) 2.3043(9); O(1) – Mn(1) – O(2) 173.72(6), N(4) – Mn(1) – Cl(1) 122.79(5).
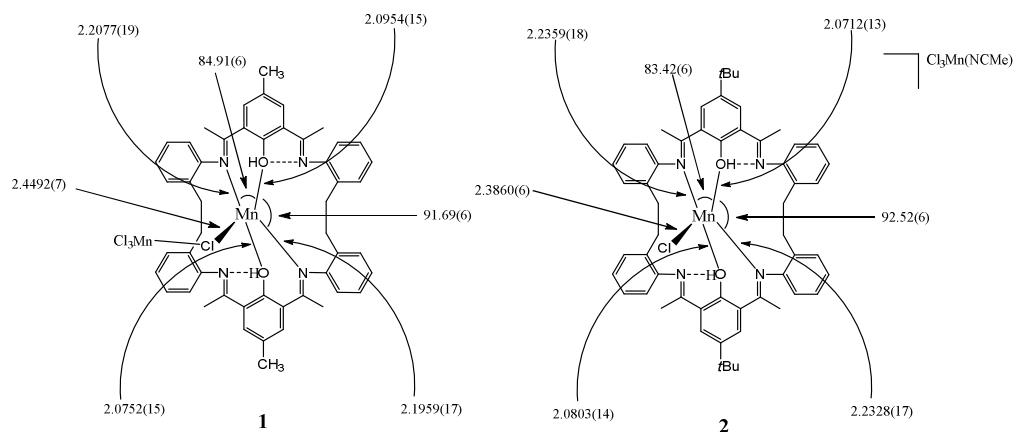
Scheme 2. Comparison of selected geometrical parameters for **1** and **2**.

Use of 2,2′-O(C6H4NH2)2

The [2 + 2] macrocycle [2,2′-O(C6H4N=CH)24-MeC6H3OH] (**II**^{R}H2), prepared from the diamine 2,2′-O(C6H4NH2)2 and [1,3-(CHO)2-5-R′C6H3OH-2] (R′ = Me, *t*Bu) in refluxing ethanol, on treatment with MnCl2 in refluxing toluene affords the yellow complexes [(MnCl)2**II**^{Me}] (**3**) or [(MnCl)2**II**^{tBu}] (**4**), respectively. The IR spectra of **3** and **4** contained a strong band at 1625 cm^{-1} assigned to v(C=N). Small crystals of **3**·C3H6O suitable for an X-ray study using synchrotron radiation were grown from acetone at ambient temperature. There is one acetone of crystallization in the asymmetric unit, which is not in contact with the Mn2 unit. The structure is shown in Figure 3 and reveals how the macrocycle is 'pinched' to accommodate coordination of the two severely distorted trigonal bi-pyramidal manganese centres. Atoms N(1)/O(3) are axial at Mn(1) and O(1)/N(3) are axial at Mn(2). The Mn – O(phenoxide) bond lengths in **3**·C3H6O [2.120(3) and 2.183(3) Å] are slightly longer than observed in **1** and **2**, but slightly shorter than those observed by Mohanta *et al*. in their mixed valence systems. [7b]
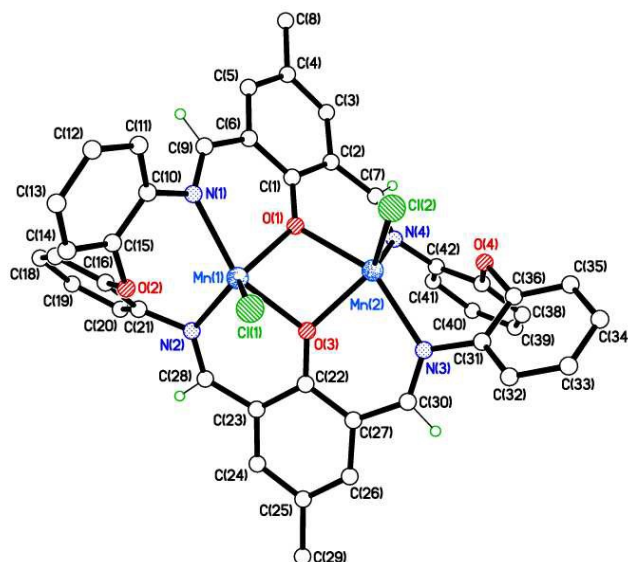
7

Figure 3. Molecular structure of $[(MnCl)_2\mathbf{II}^{Me}]\cdot C_3H_6O$ ($\mathbf{3}\cdot C_3H_6O$). Selected bond lengths (Å) and angles

(^{o}): Mn(1) – O(1) 2.120(3), Mn(1) – O(3) 2.183(3), Mn(1) – N(1) 2.206(4), Mn(1) – N(2) 2.203(4), Mn(1) –

Cl(1) 2.3464(14); O(1) – Mn(1) – O(3) 71.89(12), Mn(1) – O(1) – Mn(2) 96.22(12), N(1) – Mn(1) – N(2)

111.16(15).

If the complex is recrystallized from acetonitrile, then a different crystal system results, and in this case the

asymmetric unit contains four molecules of acetonitrile. However, the two metal complexes have similar

conformations, with chlorides on the same side in both cases (emphasized in Figure 4). The Mn –

O(phenoxide) [O(1) 2.1322(13) and 2.2384(14) Å] and Mn – N(imine) [2.2060(17) and 2.2468(17) Å]

bond lengths are as expected for Mn^{II}. [7b, 11] The aceonitrile molecules either reside in the cleft of the

molecule [those containing N(5) and N(6)] or lie between molecules (*exo*). The acetonitrile containing N(5)

also forms a weak C–H···N H-bond with C(7')–H(7') on an adjacent molecule at 2.53 Å. Molecules stack

in columns along the *a* axis via centrosymmetric weak π···π interactions between 'tolyl' rings (see Figure

S4, ESI). The Mn···Mn distances in $\mathbf{3}\cdot C_3H_6O$ and $\mathbf{3}\cdot 4MeCN$ are 3.1983(10) and 3.3347(4) Å, respectively.

8
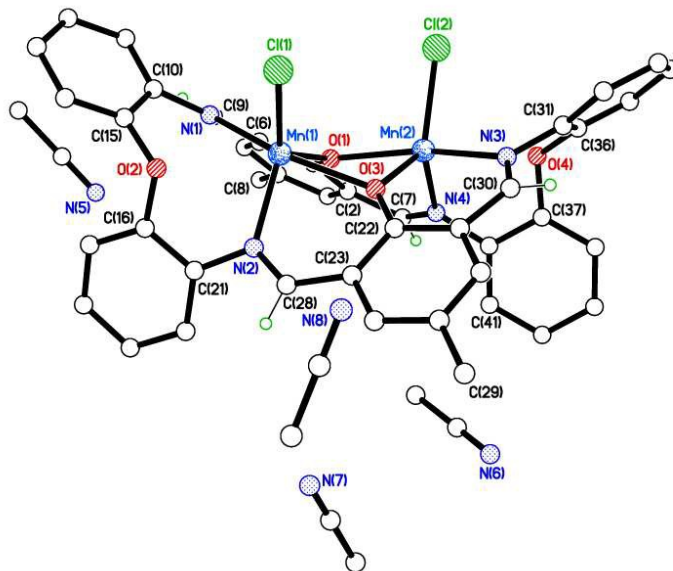
Figure 4. Molecular structure of [(MnCl)$_2$**II**^{Me}]·4MeCN (**3**·4MeCN). Selected bond lengths (Å) and angles (°): Mn(1) − O(1) 2.1322(13), Mn(1) − O(3) 2.2384(14), Mn(1) − N(1) 2.2468(17), Mn(1) − N(2) 2.2060(17), Mn(1) – Cl(1) 2.3639(6); O(1) – Mn(1) – O(3) 72.95(5), Mn(1) – O(1) – Mn(2) 101.50(6), N(1) – Mn(1) – N(2) 112.88(6).
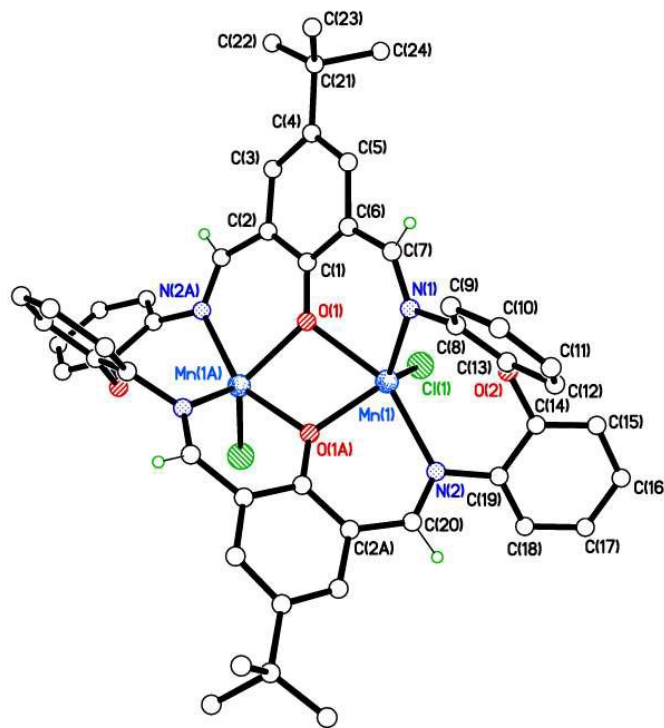
9

Figure 5. Molecular structure of [(MnCl)$_2$**II**^{tBu}] (**4**). Selected bond lengths (Å) and angles (^{o}): Mn(1) – O(1) 2.2270(17), Mn(1) – O(1A) 2.1078(15), Mn(1) – N(1) 2.193(2), Mn(1) – N(2) 2.270(2), Mn(1) – Cl(1) 2.3571(9); O(1) – Mn(1) – O(1A) 73.26(7), Mn(1) – O(1) – Mn(1A) 100.80(7), N(1) – Mn(1) – N(2) 112.92(8).

In the case of the related macrocycle derived from 2,6-diformyl-4-*tert*-butylphenol, reaction with MnCl$_2$ and similar work-up led to the isolation of the complex [(MnCl)$_2$**II**^{tBu}] (**4**) in moderate isolated yield (50 %). Crystals of **4**·MeCN suitable for an X-ray study were grown from acetonitrile at ambient temperature. The molecular structure is shown in Figure 5, with selected bond lengths and angles given in the caption. The molecule lies on a two-fold axis. The methyl groups on the *t*Bu group at C(21) are disordered over two sets of positions; major component 52.8(7) %. As for the solvates of **3**, the manganese centres in **4** adopt distorted trigonal bi-pyramidal geometries. Thus in these systems involving macrocycles of type II (see scheme 3), the two phenolate oxygens act as bridges between the two manganese ions, whilst the ether oxygen atoms do not coordinate to the metal ions. The Mn···Mn distance in **4** is 3.3408(8) Å. The MeCN of crystallisation resides in large voids between dimer complexes and was severely disordered [See X-ray Crystallography section]. Molecules stack in columns along the *b* direction (see Figure S5, ESI). The solvent-filled voids lie in layers in the *b*/*c* plane.
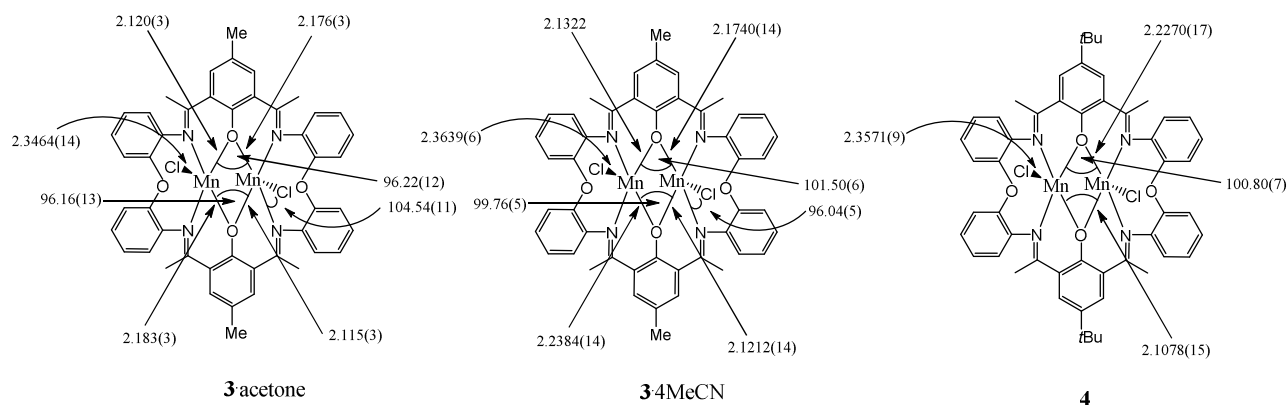
Scheme 3. Comparison of selected geometrical parameters for **3**·acetone, **3**·4MeCN and **4**.

EPR spectra for **3** and **4**, recorded as powdered samples at ambient temperature (298 K), are again dominated by broad features at g = 2.00 (for **3**) or 2.05 (for **4**) (see Figures S6 and S7, ESI). Broad features in X-band in the g = 2 region have been observed previously for dinuclear Mn(II) complexes, for example the μ-phenoxo-bis-μ-acetato complex $[(Bpmp)Mn_2(\mu\text{-}OAc)_2]^+$ (BpmpH = 2,6-bis[bis(2-pyridylmethyl)aminomethyl]-4-methylphenol). [12]

Interaction of the macrocycle **III**H_4 derived from 1,2-diaminobenzene and 5,5$^/$-di-*tert*-butyl-2,2$^/$-dihydroxy-3,3$^/$-methylenedibenzaldehyde afforded the complex $[(MnCl)_2(\textbf{III})]\cdot 2MeCN$ (**5·2MeCN**), for which small orange/brown crystals could be grown from a saturated acetonitrile solution at ambient temperature. The diffraction data were collected using synchrotron radiation. The molecular structure is shown in Figure 6. Half of the formula is unique, with the metal complex on a centre of symmetry. In this case each manganese centre is best described as adopting a square-based pyramidal geometry (*cf* trigonal bipyramidal geometries for the other complexes herein) with the chloride as the apex; each Mn centre is displaced by 0.325(3) Å out of the N_2O_2 plane. The chlorine atoms lie on opposite sides of the molecule. The Mn – O/N bonds in **5** are all significantly shorter than in the other complexes, suggesting a higher oxidation state, *i.e.* Mn(III). The Mn···Mn distance in **5** is 7.541(3) Å. In the packing of **5**, head-to-tail weak C−H···Cl interactions exist between molecules giving rise to chains along the *c* axis (see Figure 7). We note that the structure of the same complex as the water solvate $[(MnCl)_2(\textbf{III})]\cdot 3H_2O$ has recently been reported. [13] In the water solvate, the Mn centres were displaced by 0.354 Å with an Mn···Mn separation of 7.592 Å; the average Mn – O and Mn – N distances were 1.864(5) and 1.995(6) Å, respectively.

11
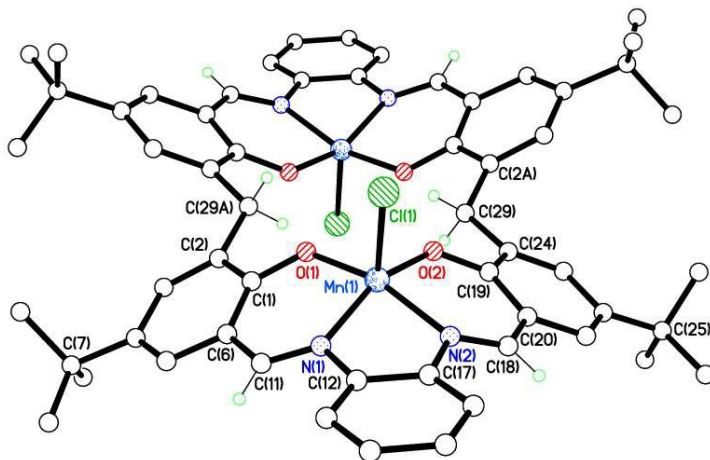
Figure 6. Molecular structure of [(MnCl)$_2$(**III**)] (**5**·2MeCN). Selected bond lengths (Å) and angles (°): Mn(1) – O(1) 1.849(4), Mn(1) – O(2) 1.871(4), Mn(1) – N(1) 1.986(4), Mn(1) – N(2) 2.000(5), Mn(1) – Cl(1) 2.379(2); O(1) – Mn(1) – O(2) 92.54(19), N(1) – Mn(1) – N(2) 81.26(19).
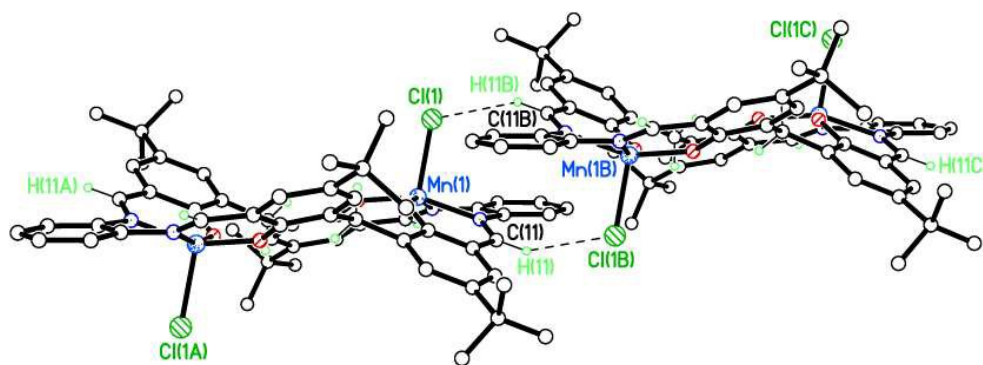
Figure 7. View of **5** showing weak, head-to-tail C–H···Cl H-bond interactions between molecules which give rise to chains along the *c* axis.

In the above macrocyclic complexes, the Mn – N bond lengths lie in the narrow range 2.178 – 2.236 Å, but with no clear pattern of variation. The Mn – O bond lengths lie in the range 2.071 – 2.238 Å, with the shortest bond lengths found in **1** and **2**, and a wider range observed in **3** and **4**. The Mn – Cl bond lengths lie in the range 2.342 – 2.386 Å when Cl is a terminal chloride ion. As expected, the bridging Cl in **1** has a longer Mn – Cl bond length. The C=N distances in structures **1 – 5** range from 1.280 – 1.310 Å and so are

insignificantly different from those of the non-coordinated C=N in **6** (see below). Indeed, the C=N

distances in range of similar solvated and non-solvated Schiff base macrocycles are slightly shorter, being

in the range 1.255 – 1.288 Å. [5b, 14] Thus, on coordination of Mn, the C=N bond lengthens by *ca*. 0.02 –

0.03 Å. A CSD search conducted on 5-coordinate Mn with a O_2N_2Cl coordination environment gave 59 hits,

[5a] for which the mean Mn – Cl = 2.370 Å indicating the values herein are typical, whilst the mean Mn – O

= 1.915 Å with a range of *ca*. 1.86 – 2.20 Å indicate the values herein are towards the higher end of those

previously reported. The search also revealed the mean Mn – N = 2.023 Å with a range of *ca*. 1.86 – 2.28 Å,

indicating that the values herein are again toward the longer end of this range. A scattergram of Mn – O

versus Mn – N distances revealed a positive correlation, so longer Mn – O distances corresponded to long

Mn – N distances – this is also the situation observed herein.

Salt complexes
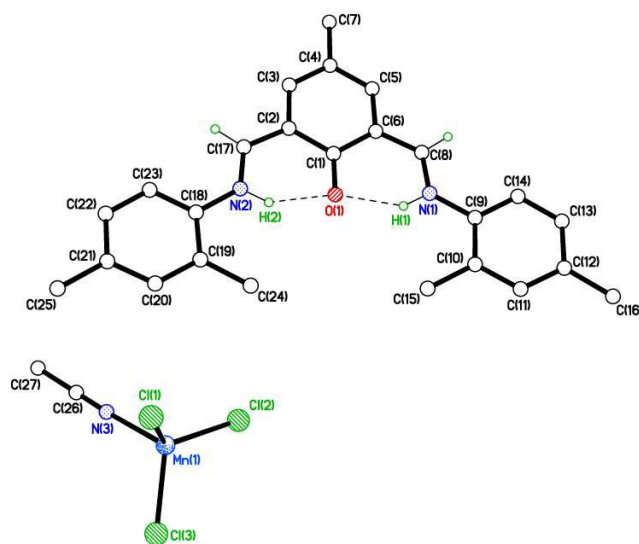
Figure 8. View of the salt **6**. Selected bond lengths (Å): Mn(1) – Cl(1) 2.3344(5), Mn(1) – Cl(2) 2.3137(5),

Mn(1) – Cl(3) 2.3295(5), Mn(1) – N(3) 2.1514(15), H(1)···O(1) 1.90(2), H(2)···O(1) 1.85(2).

For structural and catalytic comparisons, the coordination chemistry of bis(imino)phenols of type **IVH** (see

scheme 1) with manganese dichloride has also been investigated. Use of the bis(imino)phenol bearing aryl

groups at nitrogen with a 2,4-dimethyl pattern on reaction with $MnCl_2$, resulted in an ion-pair complex,

namely [2,6-(ArNHCH)$_2$-4-MeC$_6$H$_2$O][MnCl$_3$(NCMe)] (**6**) (Ar = 2,4-Me$_2$C$_6$H$_3$). Related ion-pair

complexes have been reported by Sun *et al* when using FeCl$_3$. [15] Salt **6** can be readily crystallized from

MeCN at 0 °C, and the structure is shown in Figure 8, with selected bond lengths and angles given in the

caption. In the essentially planar cation, both nitrogen atoms are involved in H-bonding to the phenolic

oxygen. The cations stack parallel to *a*, and form six weak C – H ⋯ Cl interactions with four different anions

(see Figure S9, ESI for diagram and Table S2 for details of π – π contacts).

Given in the related iron(III) chemistry, use of an aryl group bearing no *ortho* substituents results in a

complex rather than an ion-pair, [15] we attempted the same reaction using *p*-tolylamine. However, unlike

the iron case, an orange salt complex **7,** structurally different to **6**, was isolated. Single crystals were grown

from a saturated dichloromethane solution, which proved to be weakly diffracting and twinned [See X-ray

Crystallography section]. However, despite this, the structurally connectivity is clear and the salt complex

can be formulated as {[2,6-(ArNHCH)-4-Me-C$_6$H$_2$O]MnCl}$_2$[MnCl$_4$]·8CH$_2$Cl$_2$ (Ar = 4-MeC$_6$H$_4$,

7·8CH$_2$Cl$_2$). This salt lies on a two-fold axis, and so half is unique. Figure 9 reveals the nature of the

bis(chloro)-bridged dimer, in which each manganese centre is distorted octahedral, and is bound by two

protonated L type ligands each of which binds in *N,O*-bi-dentate fashion. Chloride bridging completes the

octahedral environment and in each case the bridging chlorides are *trans* to a nitrogen of a chelate; the

'free' nitrogen is involved in intramolecular H-bonding with the phenoxide oxygen within the same unique

chelate. The Mn – Cl bonds of the cation are about 2.54 Å, whilst those of the anion are *ca*. 2.36 Å; both

match examples in the CSD. [13] The Mn – O distances [*ca*. 2.09 Å] and Mn – N distances [*ca*. 2.30 Å] are

typical and consistent with the presence of Mn(II) centres. [7b, 11, 16]

14
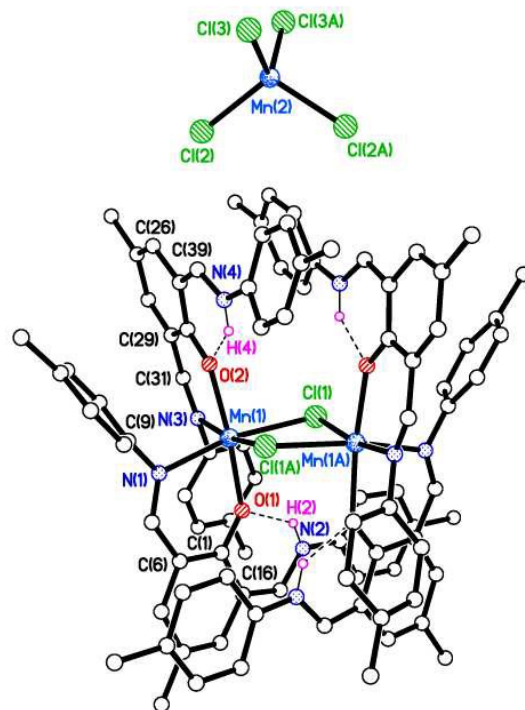
Figure 9. Molecular structure of salt complex **7**; 8 CH_2Cl_2 molecules of crystallisation omitted for clarity.

Ring opening polymerization

Complexes **1** – **7** (not **5**) have been screened for their ability to ring open polymerize ε-caprolactone in the presence of benzyl alcohol (BnOH). For comparison, the salt complexes **6** and **7** have also been investigated. Compound **2** was used to optimize the polymerization conditions and the results are presented in Table 1. Despite the good control (PDIs < 1.03), poor conversions were obtained (10.2 – 13 4 %) at all temperatures in the range 60 to 110 °C (runs 3, 6 and 7), with little advantage on prolonging the reaction time to 48 h (run 5), changing the molar ratio of ε-caprolactone to pre-catalyst/BnOH (runs 8 - 12) or even on changing the temperature. Results for **1** were similarly disappointing (runs 12 and 13); the yields and observed molecular weights (M_n) for **2** over 12 and 24 h were lower than found for **1**. The use of complexes **3** or **4** led to no isolable product. The salt complexes **6** and **7** were similarly inactive. Conducting the runs in a solvent other than toluene, such as THF or CH_2Cl_2, gave no improvement in the observed catalytic activities. In general, the resulting polymer molecular weights were much lower than expected, which

15

indicates that, in most cases, there were significant *trans*-esterification reactions occurring. However, given

the disappointing conversions observed herein, further analysis of the activity trends and resultant PCL was

not conducted. [17] We note that the use of manganese complexes as catalysts for α-olefin polymerization

has met with similar poor results. [18]

Table 1. Ring opening polymerization screening using **1 – 4**.

Run	Complex	CL: M: BnOH	T/°C	t/h	Yield/%	M_n	Mn Calc	PDI
1	2	250:1:1	110	3	13.0	440	3705	1.03
2	2	250:1:1	110	6	12.4	440	3534	1.03
3	2	250:1:1	110	12	11.2	420	3190	1.03
4	2	250:1:1	110	24	12.0	450	3420	1.02
5	2	250:1:1	110	48	13.4	450	3819	1.03
6	2	250:1:1	60	12	12.0	460	3420	1.03
7	2	250:1:1	80	12	11.4	460	3249	1.03
8	2	100:1:1	110	12	13.2	420	3762	1.03
9	2	500:1:1	110	12	12.3	410	3505	1.03
11	2	750:1:1	110	12	10.2	410	2850	1.03
12	1	250:1:1	110	12	8.20	270	2451	1.01
13	1	250:1:1	110	24	9.00	280	2565	1.02
14	3	250:1:1	110	12	_	_	_	_
15	4	250:1:1	110	12	_	_	_	_
16	6	250:1:1	110	12	_	_	_	_
17	7	250:1:1	110	24	-	-	-	

[a] By ^{1}H NMR analysis, [b] (F.W.[M]/[BnOH])(conversion), [C] Obtained from GPC analysis times 0.56

In conclusion, we have investigated the manganese coordination chemistry of a number of [2 + 2] type

Schiff-base macrocycles and find that in most cases the macrocycle has a preference for binding two

5-coordinate distorted trigonal bi-pyramidal or square pyramidal manganese centres. Related

16

bis(imino)phenols on reaction with $MnCl_2$ afford salt complexes. Application of these complexes as pre-catalysts for the ROP of ε-caprolactone was disappointing with conversions < 15 % observed at most temperatures when using **1** or **2**, whilst complexes **3** and **4** and the salt complexes were inactive. These results suggest that the combination of manganese and Schiff-base type ligation is not suited to the ROP of ε-caprolactone. Investigations into other combinations of manganese and other ligand sets are on-going in our laboratory.

Experimental

All manipulations were carried out under an atmosphere of nitrogen using standard Schlenk line and cannula techniques or a conventional N_2 filled glove box. Solvents were refluxed over the appropriate drying agents, and distilled and degassed prior to use. Elemental analyses were performed at London Metropolitan University. NMR spectra were recorded on a Varian VXR 400 S spectrometer at 400 MHz, a Gemini at 300 MHz or a Bruker DPX300 spectrometer at 300 MHz (^{1}H) and 75.5 MHz (^{13}C) at 298 K; chemical shifts are referenced to the residual protio impurity of the deuterated solvent. EPR spectroscopy was performed on an X-band ER200-D spectrometer (Bruker Spectrospin) interfaced to an ESP1600 computer and fitted with a liquid helium flow cryostat (ESR-900; Oxford Instruments), and the spectra were simulated with Simfonia. IR spectra (KBr discs) were recorded on a Perkin-Elmer 577 or 457 grating spectrophotometer. DSC analyses of polymer samples were performed on a TA Instruments DSC Q 1000. Matrix Assisted Laser Desorption/Ionization-Time Of Flight (MALDI-TOF) mass spectrometry was performed on Bruker autoflex III smart beam in linear mode. MALDI-TOF mass spectra were acquired by averaging at least 100 laser shots. 2,5-Dihydroxylbenzoic acid was used as matrix and tetrahydrofuran as solvent. Sodium chloride was dissolved in methanol and used as the ionizing agent. Samples were prepared by mixing 20 μl of polymer solution in tetrahydrofuran (2 mg/ml) with 20 μl of matrix solution (10 mg/ml) and 1 μl of a solution of ionizing agent (1 mg/ml). Then 1 ml of these mixtures was deposited on a target plate and allowed to dry in air at room temperature. The [2 + 2] macrocycles were prepared as described in

the literature. [5] All other chemicals were obtained commercially and used as received unless stated otherwise.

Synthesis of {MnCl$_4$Mn[2,2$^/$-(CH$_2$CH$_2$)(C$_6$H$_4$NH)$_2$-2,6-(4-MeC$_6$H$_3$OH)]$_2$} (**1**)

To the ligand [2,2$^/$-(CH$_2$CH$_2$)(C$_6$H$_4$N)$_2$-2,6-(4-MeC$_6$H$_3$OH)]$_2$ (0.50 g, 0.73 mmol) in toluene (30 cm^3) was added one equivalent of MnCl$_2$ (0.082 g, 0.65 mmol), and the system was refluxed for 12 h. Following removal of volatiles *in-vacuo*, the residue was extracted in MeCN (30 cm^3), affording on prolonged standing at room temperature small, orange-red crystals of **1** in 68 % yield (0.38 g). Calculated for C$_{48}$H$_{43}$Cl$_4$Mn$_2$N$_5$O$_2$·MeCN: C, 59.19; H, 4.57; N, 8.28; Found: C, 59.54; H, 4.88; N, 8.56 %. IR (cm^{-1}): 3431 (bw), 2965 (m), 2903 (w), 2806 (w), 2712 (w), 2602 (w), 2503 (w), 2247(w), 1635 (s), 1591 (m), 1540 (s), 1487 (m), 1447(w), 1401(w), 1375 (w), 1330 (w), 1299 (s), 1262 (s), 1240 (m), 1215 (m), 1184 (m), 1101 (s), 1106 (s), 1023 (s), 873 (w), 803 (s), 758 (s), 701 (m), 671 (m), 597 (w), 574 (w), 534 (w), 502 (w), 468(w), 451 (w); MS (E.I.): 914.76 [M-CH$_3$]$^+$, EPR (X-band, solid, 110 K): g = 2.00.

Synthesis of {MnCl$_4$Mn[2,2$^/$-(CH$_2$CH$_2$)(C$_6$H$_4$NH)$_2$-2,6-(p-*t*-BuC$_6$H$_3$O)]$_2$} (**2**)

As for **1**, but using {[1,2-(N)$_2$C$_6$H$_4$]CH[CH$_2$(p-*t*-BuC$_6$H$_2$OH)]}$_2$ (0.50 g, 0.65 mmol) and MnCl$_2$ (0.082 g, 0.65 mmol) affording **2** as orange/red blocks, 54 % yield (0.36 g). Calculated for C$_{53}$H$_{53}$Cl$_4$Mn$_2$N$_4$O$_2$·CH$_3$CN: C, 61.32; H, 5.24; N, 6.62; Found: C, 61.24; H, 5.31; N, 6.75 %. IR (cm^{-1}): 3412 (bm), 3053 (w), 2953 (m), 2866 (w), 1634 (s), 1587 (m), 1537 (s), 1503 (w), 1484 (m), 1461 (w), 1397 (w), 1361 (w), 1331 (w), 1241 (m), 1182 (m), 1102 (w), 1058 (w), 1022 (m), 885 (w), 862 (w), 828 (w), 794 (w), 757 (m), 688 (w), 624 (w), 596 (w), 573 (w), 537 (w), 494 (w), 475 (w); MS (E.I.): 1016 [M]$^+$, EPR (X-band, solid, 110 K): g = 2.04.

Synthesis of [(MnCl)$_2$ 2,2$^/$-O(C$_6$H$_4$N=CH)$_2$4-MeC$_6$H$_3$O] (**3**)

As for **1**, but using [2,2$^{/}$-O(C$_6$H$_4$N=CH)$_2$4-MeC$_6$H$_3$OH] (L$^{/}$H$_3$) (0.5 g, 0.76 mmol) and MnCl$_2$ (0.19 g, 1.5

mmol) affording **3** as orange/red blocks, 54 % yield (0.35 g). The complex can be recrystallized from either

acetone or acetonitrile. Calculated for C$_{44}$H$_{36}$Cl$_2$Mn$_2$N$_4$O$_4$·CH$_3$CN (sample dried *in-vacuo* for 2 h,

–3MeCN): C, 60.94; H, 4.34; N, 7.06; Found: C, 60.61; H, 3.99; N, 7.36 %. IR (cm^{-1}): 3435 (bm), 3057 (w),

2958 (w), 2867 (w), 1625 (s), 1592 (s), 1537 (s), 1486 (m), 1454 (m), 1396 (m), 1362 (w), 1341 (w), 1318

(w), 1238 (w), 1221 (s), 1181 (m), 1109 (m), 1057 (w), 1024 (s), 983 (w), 935 (w), 893(w), 865w (w), 838

(w), 798 (m), 777 (w), 757 (w), 701 (w), 669 (w), 631(w), 568 (w), 517 (w), 469 (w), 454 (w); MS (E.I.):

848.25 [M]$^+$. EPR (X-band, solid, 298 K): 2.00.

Synthesis of [(MnCl)$_2$ 2,2$^{/}$-O(C$_6$H$_4$N=CH)$_2$4-*t*-BuC$_6$H$_3$O] (**4**)

As for **1**, but using {[2,2$^{/}$-O(C$_6$H$_4$N=CH)$_2$4-*t*-BuC$_6$H$_3$OH] (0.5 g, 0.67 mmol) and MnCl$_2$ (0.17 g, 1.35

mmol) affording **4** as orange/red blocks, yield 50 % (0.31g). Calculated for C$_{50}$H$_{48}$Cl$_2$Mn$_2$N$_4$O$_4$: C, 63.23;

H, 5.09; N, 5.90; Found: C, 63.10; H, 5.06; N, 6.16 %. IR (cm^{-1}): 3428 (bs), 3057 (w), 2964 (w), 2905(w),

1625 (s), 1593 (s), 1541 (s), 1484 (s), 1450 (s), 1395 (m), 1340 (m), 1237 (m), 1215 (s), 1180 (m), 1106 (m),

1065 (m), 1035 (m), 937 (w), 860 (w), 837 (m), 802 (m), 755 (m), 713 (w), 566 (w), 511 (w), 475 (w); MS

(E.I.): 932.51[M]$^+$. EPR (X-band, solid, 298 K): 2.05.

Synthesis of [(MnCl)$_2$(**III**)]·2MeCN (**5**·2MeCN).

To a Schlenk flask containing ligand **III**H$_4$ (1.00 g, 1.13 mmol) and MnCl$_2$ (0.29 g, 2.3 mmol) was added

toluene (30 ml) and the system was then refluxed for 12 h. On cooling, volatiles were removed and the

residue was extracted into warm acetonitrile (20 ml). Small orange/brown prisms formed on prolonged

standing (2 to 3 days) at ambient temperature. Yield 0.85 g, 71 %. Calculated for

C$_{58}$H$_{60}$Cl$_2$Mn$_2$N$_4$O$_8$·2MeCN: C, 65.32; H, 5.84; N, 7.37; Found: C, 65.14; H, 5.77; N, 7.46 %. IR (cm^{-1}):

2308w, 2279w, 1651w, 1604m, 1596m, 1575m, 1539w, 1316m, 1261s, 1193m, 1094bs, 1022bs, 876w,

801s, 768w, 742m, 722m. MS (E.I. positive): 1098.9 **5**·MeCN, 1022.4 **5** – Cl. M.S. (solid, APCI, ASAP)

[19]: 1098.9 **5**·MeCN, 1057.9 **5**.

Synthesis of [2,6-(ArNHCH)$_2$-4-MeC$_6$H$_2$O][MnCl$_3$(NCMe)] (**6**) (Ar = 2,4-Me$_2$C$_6$H$_3$).

As for **1**, but using 2,6-(2,4-Me$_2$C$_6$H$_3$NCH)$_2$-4-MeC$_6$H$_2$OH (1.00 g, 2.70 mmol) and MnCl$_2$ (0.34 g, 2.7

mmol) affording **6** as red prisms, 79 % (1.22 g). Calculated for C$_{27}$H$_{30}$Cl$_3$MnN$_3$O : C, 56.51; H, 5.27; N,

7.32; Found: C, 56.99; H, 5.29; N, 7.54 %. IR (cm^{-1}): 3361 (w), 2358 (w), 2295 (w), 2268 (w), 2242 (w),

1627 (s), 1595 (s), 1538 (s), 1313 (s), 1282 (s), 1262 (s), 1234 (m), 1201 (m), 1170 (m), 1148 (m), 1115 (m),

1060 (m), 1030 (m), 987 (m), 928 (w), 897 (m), 877 (w), 857 (w), 820 (m), 812 (w), 722 (s), 661 (w); MS

(nanoelectrospray): 371.2 (cation + H).

Synthesis of {[2,6-(ArNHCH)$_2$-4-Me-C$_6$H$_2$O]MnCl}$_2$[MnCl$_4$]·8CH$_2$Cl$_2$ (**7**·8CH$_2$Cl$_2$) (Ar = 4-MeC$_6$H$_4$).

As for **1**, but using 2,6-(4-MeC$_6$H$_4$NCH)$_2$-4-MeC$_6$H$_2$OH (0.92 g, 2.7 mmol) and MnCl$_2$ (0.34 g, 2.7 mmol)

affording **7** as red prisms on crystallization from either dichloromethane or acetonitrile, 89 % (1.31 g).

Calculated for C$_{92}$H$_{88}$Cl$_6$Mn$_3$N$_8$O$_4$·CH$_2$Cl$_2$ (sample dried for 1 h *in-vacuo*): C, 60.96; H, 4.95; N, 6.12;

Found: C, 61.36; H, 4.90; N 6.83 %. IR (cm^{-1}): 2243 (w), 1632 (s), 1593 (s), 1533 (s), 1340 (s), 1319 (s),

1278 (s), 1262 (s), 1229 (m), 1211 (m), 1195 (m), 1107 (m), 1061 (m), 1016 (m), 991 (m), 897 (w), 880 (w),

847 (w), 834 (m), 820 (w), 779 (w), 722 (s), 703 (w), 689 (w), 661 (w), 590 (w), 546 (w), 516 (m), 494 (m);

MS (nanoelectrospray): 1137 (salt – anion – 2LH - 2Cl), 1104 (salt – L – *p*-tolylN).

Ring opening polymerization. Typical polymerization procedures in the presence of one equivalent of

benzyl alcohol (Table 4, run 1) are as follows. A toluene solution of **2** (0.010 mmol, in 1.0 mL toluene) and

BnOH (0.010 mmol) were added into a Schlenk tube in the glove-box at room temperature. The solution

was stirred for 2 min, and then ε-caprolactone (2.5 mmol) along with 1.5 mL toluene was added to the

solution. The reaction mixture was then placed into an oil bath pre-heated to the required temperature, and

the solution was stirred for the prescribed time. The polymerization mixture was then quenched by addition

of an excess of glacial acetic acid (0.2 mL) into the solution, and the resultant solution was then poured into

methanol (200 mL). The resultant polymer was then collected on filter paper and was dried *in* vacuo.

X-ray Crystallography

Diffraction data were collected on CCD area detector diffractometers: Bruker SMART 1K for **1**·3MeCN,

3·C_2H_6O, Agilent Xcalibur EOS for **2**, **3**·4MeCN, **4**·MeCN, Bruker APEX II for **5**·2MeCN and **6**. [20] Full

details are presented in Table 5. Data were corrected for absorption and Lp effects. Synchrotron radiation at

Daresbury Laboratory Station 9.8 was used for **1**·3MeCN, **3**·C_2H_6O, and **5**·2MeCN. Structures were solved

by direct or iterative methods and refined by full-matrix least squares on F^2. [21] For **2** the methyl groups on

*t*Bu group at C(22) were modelled as disordered over two sets of positions with major component 60(3) %.

For **4**·MeCN the methyl groups on *t*Bu group at C(21) were modelled as disordered over two sets of

positions with major component 52.8(7) % and the MeCN of crystallisation was modelled as a diffuse area

of electron density by the Platon 'Squeeze' procedure due to severe disorder. [22] For **5**·2MeCN the *t*Bu

group at C(7) was modelled as disordered over two sets of positions with major component 56.0(18) %.

Provisional crystal data for **7**·8 CH_2Cl_2: orange crystals, orthorhombic, space group *Pbcn*, unit cell: $a =$

25.057(3), $b = 18.987(2)$, $c = 24.022(3)$, V = 11429(4) $Å^3$, crystal size 1.36 × 0.48 × 0.19 mm^3, $T = 150K$.

Four unique CH_2Cl_2 solvent molecules of crystallisation; one of these four was modelled by the Platon

'Squeeze' procedure [22]; all show evidence of disorder. The crystals desolvated rapidly and the apparent

twinning could not be resolved.

CCDC 1415950-1415956 contain the supplementary crystallographic data for this paper. These data can be

obtained free of charge from The Cambridge Crystallographic Data Centre via

www.ccdc.cam.ac.uk/data_request/cif.

21

References

[1] I. Bratko and M. Gómez, *Dalton Trans*. **2013**, *42*, 10664-10681 and references therein.

[2] S. Anbu, M. Kandaswamy, P. Suthakaran, V. Murugan and B. Varghese, *J. Inorg. Biochem*. **2009**, *103*, 401-410.

[3] (a) N. H. Pilkington and R. Robson, *Aust. J. Chem*. **1970**, *23*, 2225-2236. (b) M. Bell, A.J. Edwards, B. F. Hoskins, E. H. Kachab and R. Robson, *J. Am. Chem. Soc*. **1989**, *111*, 3603-3610; (c) B. Bosnich, *Inorg. Chem*. **1999**, *38*, 2554-2562; (d) S. R. Koruoju, N. Mangayarkarasi, S. Ameerunisha, E. J. Valente and P. S. Zacharias, *Dalton Trans*. **2000**, 2845-2852; (e) U. Casellato, S. Tamburini, P. Tomasin and P. Vigato, *Inorg. Chimica Acta*, **2004**, *357*, 4191; (f) W. Huang, H. -B. Zhu and S. -H. Guo, *Coord.Chem. Rev*. **2006**, *250*, 414-423; (g) P. A. Vigato, S.Tamburini and L. Bertolo, *Coord.Chem. Rev*. **2007**, *251*, 1311-1492; (h) V. Lozan, C. Loose, J. Kortus and B. Kersting, *Coord.Chem. Rev*. **2009**, *253*, 2244-2260.

[4] A. Arbaoui, C. Redshaw and D. L. Hughes, *Chem. Commun*. **2008**, 4717-4720.

[5] (a) F. H. Allen, *Acta Cryst.*, **2002**, *B58*, 380; (b) For **I**H_2 see A. Arbaoui, C. Redshaw and D. L. Hughes. *Supramol. Chem*. **2009**, *21*, 35-43.

[6] About a third of the structures are acetate bridged species and around 20 % are high nuclearity manganese complexes.

[7] See for example, (a) K. S. Banu, T. Chattopadhyay, A. Banerjee, M. Mukherjee, S. Bhattacharya, G. K. Patra, E. Zangrando and D. Das, *Dalton Trans*. **2009**, *40*, 8755-8764. (b) A. Jana, N. Aliaga-Alcalde, E. Ruiz and S. Mohanta, *Inorg. Chem*. **2013**, *52*, 7732–7746.

[8] J. R. Anacona, E. Bastardo and J. Camus, *Transition metal chem.* **1999**, *24*, 478-480.

[9] Q. -H. Xia, H .-Q. Ge, C. -P. Ye, Z. -M. Liu, and K. -X. Su, *Chem. Rev*. **2005**, *105*, 1603 – 1662.

[10] B. B. Idage, S. B. Idage, A. S. Kasegaonkar and R. V. Jadhav, *Materials Science and Engineering B*, **2010**, *168*, 193–198.

[11] (a) J. -C. Jiang, Z. -L. Chu, W. Huang, G. Wang and X. -Z. You, *Inorg. Chem*. **2010**, *49*, 5897-5911. (b) R. Golbedaghi, S. Salehzadeh, H. R. Khavasi and A. G. Blackman, *Polyhedron*, **2014**, *68*, 151-156.

[12] S. Blanchard, G. Blondin, E. Rivière, M. Nierlich and J. -J. Girerd, *Inorg. Chem*. **2003**, *42*, 4568-4578.

[13] P. Biswas, P. Bag, A. K. Dutta, U. Flörke and K. Nag, *Polyhedron*, **2014**, *75*, 113 – 126.

[14] W. Yang, K. -Q. Zhao, T. J. Prior, D. L. Hughes, A. Arbaoui, T. Bian, Y. Chao, M. R. J. Elsegood and C. Redshaw , unpublished results.

[15] L. Han, J. Du, H. Yang, H. Wang, X. Leng, A. Galstyan, S. Zarić and W. -H. Sun, *Inorg. Chem. Comm*. **2003**, *6*, 5 - 9.

[16] A search of the CSD for the $[MnO_2N_2Cl]_2$ core afforded 4 hits: (a) M. A. S. Goher, M. A. M. Abu-Youssef, F. A. Mautner and A. Popitsch, *Polyhedron* **1993**, *12*, 1751-1756. (b) S. Onaka, L. Hong, M. Ito, T. Sunahara, H. Imai and K. Inoue, *J. Coord. Chem*. **2005**, *58*, 1523-1530. (c) J. -W. Zhang, H. -S. Wang and Y. Song, *Inorg. Chem. Comm*. **2011**, *14*, 56-60. (d) M. Alexandru, M. Cazacu, A. Arvinte, S. Shova, C. Turta, B. C. Simionescu, A. Dobrov, E. C. B. A. Alegria, L. M. D. R. S. Martins, A. J. L. Pombeiro and V. B. Arion, *Eur. J. Inorg. Chem*. **2014**, 120-131. (e) CSD system: F. H. Allen, *Acta Cryst*., **2002**, *B58*, 380-388.

[17] These complexes were also found to be inactive as catalysts for benzene oxidation using hydrogen peroxide, X. Liu, L. Wu, X. Wang, K. -Q. Zhao and C. Redshaw, unpublished results.

[18] S. Blanchard, G. Blondin, E. Rivière, M. Nierlich and J. -J. Girerd, *Inorg. Chem*. **2003**, *42*, 4568-4578 and references therein.

[19] APCI refers to the ionization method, Atmospheric Pressure Chemical Ionization, in which samples introduced into the APCI source via an Atmospheric Solids Analysis Probe (ASAP) are vaporized then ionized using a corona discharge ($\sim 4\mu A$). The benefit of using ASAP is that samples can be introduced at ambient temperature as solids or in solution, then the temperature in the source is increased until the sample vaporizes.

[20] (a) SMART, SAINT, and APEX 2 software for CCD diffractometers. (1997-2012). Bruker AXS Inc., Madison, USA. (b) Agilent (2013). CrysAlis PRO. Agilent Technologies, Yarnton, Oxfordshire, England.

[21] (a) G.M. Sheldrick, *Acta Cryst*. **2015**, *C71*, 3-8. (b) L. Palatinus and G. Chapuis, *J. Appl. Cryst.* **2007**, *40*, 786-790.

[22] (a) A. L. Spek, *Acta Crystallogr*. **1990**, *A46*, C34. (b) P. v. d. Sluis and A. L. Spek, *Acta Cryst*allogr. **1990**, *A46*, 194.

Table 5.　　　Crystallographic data for complexes **1**·3MeCN, **2** and **3**·C_3H_6O.

Compound	1	2	3·C_3H_6O
Formula	$C_{46}H_{40}N_4O_2Mn_2Cl_2 \cdot 3CH_3CN$	$[C_{52}H_{52}N_4O_2MnCl][C_2H_3NCl_3Mn]$	$C_{42}H_{30}N_4O_4Mn_2Cl_2 \cdot C_3H_6O$
Formula weight	1055.66	1057.71	893.56
Crystal system	Triclinic	Triclinic	monoclinic
Space group	$P\bar{1}$	$P\bar{1}$	$P2_1/c$
Unit cell dimensions			
a (Å)	11.2704(15)	10.7462(3)	11.3736(14)
b (Å)	11.895(2)	12.3269(5)	14.4597(18)
c (Å)	20.373(4)	21.8883(7)	26.105(3)
α (°)	106.635(10)	84.265(3)	90
β (°)	94.676(12)	89.403(2)	100.577(3)
γ (°)	103.633(13)	66.420(3)	90
V (Å^3)	2510.4(8)	2642.70(17)	4220.3(9)
Z	2	2	4
Temperature (K)	160(2)	293	160(2)
Wavelength (Å)	0.6942	0.71073	0.6931
Calculated density (g.cm^{-3})	1.397	1.329	1.406
Absorption coefficient (mm^{-1})	0.71	0.72	0.72
Transmission factors (min./max.)	0.934 and 0.977	0.931 and 1.000	0.938 and 0.986

Crystal size (mm^3)	$0.09 \times 0.04 \times 0.03$	$0.40 \times 0.30 \times 0.20$	$0.09 \times 0.06 \times 0.02$
θ(max) (°)	29.3	29.2	26.0
Reflections measured	17406	25184	22979
Unique reflections	12080	12137	8858
R_{int}	0.020	0.028	0.115
Reflections with $F^2 > 2\sigma(F^2)$	9383	8754	4928
Number of parameters	615	642	528
$R_1 [F^2 > 2\sigma(F^2)]$	0.046	0.046	0.071
wR_2 (all data)	0.119	0.114	0.169
GOOF, S	1.00	1.05	0.90
Largest difference peak and hole (e $Å^{-3}$)	0.52 and −0.54	0.46 and −0.45	1.17 and −1.20

25

Table 5 con't.   Crystallographic data for complexes **3**·4MeCN, **4**, **5**·2MeCN and **6**.

Compound	3·4MeCN	4	5·2MeCN	6
Formula	$C_{42}H_{30}N_4O_4Mn_2Cl_2 \cdot 4C_2H_3N$	$C_{48}H_{42}N_4O_4Mn_2Cl_2 \cdot C_2H_3N$	$C_{58}H_{60}N_2O_4Mn_2Cl_2 \cdot 2C_2H_3N$	$[C_{25}H_{27}Cl_2N_2O][C_2H_3NMnCl_3]$
Formula weight	999.69	960.69	1139.98	573.83
Crystal system	Triclinic	Monoclinic	Triclinic	Monoclinic
Space group	$P\bar{1}$	$P2/c$	$P\bar{1}$	$C2/c$
Unit cell dimensions				
a (Å)	9.0678(3)	13.5740(14)	9.251(3)	8.6706(4)
b (Å)	14.5779(6)	9.1261(11)	12.594(4)	23.5547(10)
c (Å)	18.8111(7)	22.833(3)	12.781(4)	27.6317(12)
α (°)	72.522(3)	90	82.736(5)	90
β (°)	83.680(3)	102.45(1)	83.976(5)	97.6782(7)
γ (°)	87.859(3)	90	70.543(5)	90
V (Å³)	2357.39(16)	2762.0(6)	1389.6(8)	5592.7(4)
Z	2	2	1	8
Temperature (K)	143	293	120(2)	120(2)
Wavelength (Å)	0.71073	0.71073	0.6897	0.71073
Calculated density (g.cm⁻³)	1.408	1.155	1.362	1.363
Absorption Coefficient t(mm⁻¹)	0.70	0.60	0.55	0.78
Transmission factors (min./max.)	0.909 and 1.000	0.909 and 1.000	0.937 and 0.984	0.811 and 0.926
Crystal size (mm³)	$0.30 \times 0.25 \times 0.20$	$0.30 \times 0.20 \times 0.20$	$0.12 \times 0.08 \times 0.03$	$0.28 \times 0.15 \times 0.10$
θ(max) (°)	29.0	29.1	24.0	30.5
Reflections measured	22126	13163	10273	33498
Unique reflections	10861	6314	4710	8544
R_{int}	0.027	0.055	0.056	0.033
Reflections with $F^2 > 2\sigma(F^2)$	8698	3892	3112	6516
Number of parameters	601	294	383	330
$R_1 [F^2 > 2\sigma(F^2)]$	0.041	0.053	0.084	0.037
wR_2 (all data)	0.094	0.118	0.273	0.101
GOOF, S	1.05	0.92	1.06	1.01
Largest difference peak and hole (e Å⁻³)	0.43 and -0.29	0.41 and –0.48	0.69 and –0.72	0.42 and –0.29